Clim Dyn (2014) 42:1097–1111
DOI 10.1007/s00382-013-1844-3

High and low latitude types of the downstream influences of the North Atlantic Oscillation

Jie Song · Chongyin Li · Wen Zhou

Received: 8 October 2012 / Accepted: 10 June 2013 / Published online: 18 June 2013

Abstract Using reanalysis data, we find that the downstream-propagating quasi-stationary Rossby wave train associated with the North Atlantic Oscillation (NAO) generally propagates along a high (low)-latitude pathway during warm (cold) El Niño-Southern Oscillation (ENSO) boreal winters. Consistent with the different propagation directions of the NAO-related downstream wave train, during the warm (cold) ENSO winters, the NAO is associated with significant 300 hPa geopotential height anomalies over eastern Siberia (the Arabian Sea, the east coast of Asia at around 40°N, and the North Pacific), and the near-surface air temperature perturbations associated with the NAO over the high latitudes of Asia are relatively strong (weak). Based on these differences, we argue that the NAO has two distinct types of downstream influence: a high-latitude type and a low-latitude type. Furthermore, we argue that the two types of NAO's downstream influence are modulated by the intensity of the subtropical potential vorticity (PV) meridional gradient over Africa. When this gradient is weak (strong), as in the warm (cold) ENSO winters, the NAO's downstream influence tends to be of the high (low)-latitude type. These results are further supported by analysis of intraseasonal NAO events. We separate NAO events into two categories in terms of the intensity of the subtropical PV gradient over Africa. Composites of the NAO events accompanied by a weak (strong) subtropical PV gradient show that the NAO-related downstream wave train tends to propagate along a high (low)-latitude pathway.

Keywords North Atlantic Oscillation · Downstream influence · Asian jet waveguide · Reflective wave · ENSO

J. Song (✉) · C. Li
LASG, Institute of Atmospheric Physics (IAP), Chinese Academy of Sciences, P. O. BOX 9804, Beijing 100029, China
e-mail: song_jie@mail.iap.ac.cn

W. Zhou
Guy Carpenter Asia–Pacific Climate Impact Centre, School of Energy and Environment, City University of Hong Kong, Hong Kong, China

1 Introduction

The North Atlantic Oscillation (NAO), which refers to a seesawing of atmospheric mass between the Arctic and the subtropical Atlantic, is recognized as the regionally dominant mode of atmospheric circulation variability over the North Atlantic (e.g., Van Loon and Rogers 1978; Barnston and Livezey 1987; Hurrell et al. 2003). However, it has a dramatic influence on surface temperature variability over the entire Northern Hemisphere (NH), especially in boreal winters. During winters when the NAO index is positive, the eastern Canadian Arctic and Greenland are colder than normal, while North America and the broad high-latitude region of the entire Eurasian continent experience warmer than normal conditions, and vice versa (Van Loon and Rogers 1978; Hurrell 1995, 1996; Greatbatch 2000, Marshall et al. 2001). Based on 60 years of data from 1935 to 1995, Hurrell (1996) estimated that the NAO accounts for more than one-third of the variance in the hemispheric winter surface temperature north of 20°N.

From winter surface temperature anomalies corresponding to variations in the NAO (for example, see Fig. 3 in Hurrell 1996), a remarkable feature is apparent: the NAO has a strong influence on surface temperatures in regions far downstream (such as the Asian continent) as in western Europe, indicating that a coherent NAO signal in the anomalous surface temperatures extends all the way

across Eurasia from the Atlantic to the Pacific. It is known that the NAO is associated with a pulsing of the Atlantic storm track and a meridional displacement of the midlatitude jet over the Atlantic (e.g., Wettstein and Wallace 2010). The positive (negative) phase of the NAO is accompanied by enhanced (reduced) storm track activity over the North Atlantic and a simultaneous poleward (equatorward) shift of the midlatitude Atlantic jet. One might expect that the anomalous warm (cold) surface temperatures over Eurasia during the positive (negative) phase of the NAO are due to the enhanced (reduced) activity of transient eddies and their downstream propagation. However, Hurrell and Van Loon (1997) showed that the effect of anomalous transient eddies on the temperature perturbation is confined to the North Atlantic/European sector and, more importantly, these eddies act to oppose the low-level temperature perturbation associated with the NAO. Therefore, their results indicate that the zonal advection of the climatological temperature gradient by the anomalous westerly flow associated with the NAO induces the temperature perturbation over the downstream regions of the NAO (see also Trigo et al. 2002; in this study, the "downstream regions of the NAO" denotes the Eurasian continent, 0°–120°E). However, since the anomalous westerlies associated with the NAO are regionally confined to the North Atlantic and Europe, the anomalous warm or cold temperatures cannot be advected deep into Eurasia. Therefore, the horizontal temperature advection mechanism may not explain the temperature variations associated with the NAO in regions far downstream. The NAO must work in combination with other processes to exert its influences on such regions.

To explain the extension of the NAO's influence over regions far downstream, a mechanism called the "Asian jet waveguide-trapped wave train" (also known as the "NAO-related circumglobal teleconnection") has been proposed in some studies (Branstator 2002; Watanabe 2004), which have argued that the Asian jet acting as a waveguide (Hoskins and Ambrizzi 1993) can extend the influences of the NAO over regions far downstream by trapping the downstream-propagating quasi-stationary Rossby wave train associated with the NAO (e.g., the NAO-related downstream wave train). However, in our opinion, the "Asian jet waveguide-trapped wave train" mechanism is insufficient to explain the downstream influences of the NAO. At least, this mechanism cannot explain the surface temperature anomalies associated with the NAO over the high latitudes of Asia. This is because the Asian jet waveguide-trapped wave train is primarily confined to the subtropical latitudes, as shown in Figs. 3 and 13 in Watanabe (2004). Then how can we use this subtropical quasi-stationary Rossby wave train to explain the surface temperature anomalies associated with the NAO over the high latitudes of Asia? In fact, Li et al. (2008) found that there is a teleconnection pattern extending from the North Atlantic to East Asia along a high-latitude pathway over Eurasia. However, they detected this teleconnection only during the month of March. Some studies have shown that there are high-latitude wave trains propagating along the northern storm track branch upstream of the Pacific storm track over the northern Eurasian continent (Chang and Yu 1999; Lee 2000).

Based on the above discussion and the results of previous studies, we hypothesize that the NAO should have a high-latitude pathway in addition to the subtropical Asian jet waveguide pathway in order to spread its influences over regions far downstream. In this study, we use reanalysis data to investigate whether a high-latitude pathway and a low-latitude pathway (i.e., the subtropical Asian jet pathway) exist. We call these two pathways the high-latitude type (the H type hereafter) and the low-latitude type (the L type hereafter). These different pathways appear to produce different downstream influences of the NAO. Accordingly, the NAO associated with the H(L) type pathway is referred to as the H(L) type of NAO.

We find that the so-called H and L types of NAO are evident in warm and cold El Niño-Southern Oscillation (ENSO) boreal winters (December–February, DJF), respectively (details are given in Sect. 3). ENSO, the dominant pattern of interannual tropical climate variability, has significant influences around the globe (e.g., Trenberth et al. 1998). Many observational and modeling studies have indicated that the surface signal of El Niño (La Niña) events in late winter in the North Atlantic-European region appears as a projection onto a negative (positive) phase of the NAO, and the negative (positive) NAO phase occurs more frequently in late winter during El Niño (La Niña) events (e.g., Pozo-Vázquez et al. 2001; Moron and Plaut 2003; Gouirand and Moron 2003; Melo-Goncalves et al. 2005; Brönnimann et al. 2007; Gouirand et al. 2007; Li and Lau 2012). Müller and Roeckner (2006) suggested that this kind of linkage between ENSO and the NAO could become stronger in the future. In addition, Song et al. (2011) found that ENSO can also impact the zonal pattern of the NAO.

The rest of this paper demonstrates and discusses our results in detail, organized as follows: In Sect. 2, we describe the data and analysis methods used in this study. In Sect. 3, we use monthly mean data to show and compare NAO-related circulation anomalies and downstream wave trains during the warm and cold ENSO winters to demonstrate the existence of the H and L type pathways. Ratios of the H and L types of NAO during strong positive and negative NAO days are also roughly investigated and discussed. We also discuss the possible role of the intensity of the subtropical potential vorticity (PV) gradient over Africa in modulating the pathways of the NAO's downstream

influence. In order to further verify the existence of the two pathways, we use daily data to identify the two types of NAO in intraseasonal NAO events. Finally, Sect. 4 provides conclusions and further discussion.

2 Data and methods

2.1 Data

The primary data set used in this study is the National Centers for Environmental Prediction/National Center for Atmospheric Research (NCEP/NCAR) reanalysis-1 monthly and daily data (Kalnay et al. 1996). In this study, we use sea level pressure (SLP), near-surface air temperature (SAT, at the 0.995 sigma level), zonal wind, meridional wind, and geopotential height at the 300 hPa level. The NCEP/NCAR data cover the time period from January 1948 to December 2009. Because PV fields are not included in the NCEP/NCAR reanalysis-1 data and they are available in the European Center for Medium-Range Weather Forecasting (ECMWF) ERA-40 reanalysis data (Uppala et al. 2005), in the PV-related analysis of this study, we use the ECMWF ERA-40 monthly and daily data instead. The ERA-40 data cover the time period from September 1957 to August 2002. In this study, we restrict our investigation to the DJF. The horizontal resolution of the data is 2.5° × 2.5°.

In this study, we use the monthly Niño 3.4 index, which is downloaded from the website of the Climate Analysis Section within the Climate and Global Dynamics Division of the NCAR Earth System Laboratory, to select the warm and cold boreal winters of ENSO. The criterion is half of the standard deviation of winter-averaged values of the Niño 3.4 index. Of the 61 winters (1948/1949–2008/2009), 19 are warm ENSO winters and 21 are cold ENSO winters (listed in Table 1).

2.2 Analysis methods

In this study, we use linear regression and composite analysis. The monthly (daily) NAO indices are defined as the first principal component (PC1) of the DJF monthly (daily) SLP anomalies over the Atlantic region (20°–85°N, 90°W–50°E). Before the Empirical Orthogonal Function analysis, the data were weighted by the square root of the cosine of the latitude to account for the decrease in grid area toward the pole. The NAO patterns acquired using the monthly and daily data are almost identical. For the monthly (daily) data, anomalies are defined as a deviation from the seasonal cycle, which is defined as the long-term mean of each calendar month (day). In our composite analysis of the time evolution of intraseasonal NAO events, a Lanczos 10-day low-pass filter with 31 weights is applied to daily 300 hPa meridional wind anomalies in order to remove noisy transient synoptic disturbances.

Table 1 The warm and cold ENSO winters from 1948/1949 to 2008/2009

Warm ENSO winters (19)	51/52, 57/58, 63/64, 65/66, 68/69, 69/70, 72/73, 76/77, 77/78, 79/80, 82/83, 86/87, 87/88, 91/92, 94/95, 97/98, 02/03, 04/05, 06/07
Cold ENSO winters (21)	49/50, 50/51, 54/55, 55/56, 64/65, 67/68, 70/71, 71/72, 73/74, 75/76, 83/84, 84/85, 85/86, 88/89, 95/96, 98/99, 99/00, 00/01, 05/06, 07/08, 08/09

3 Analysis results

3.1 The NAO in the warm and cold ENSO winters

To demonstrate the existence of the two types of downstream influence of the NAO, we begin our analysis by showing and discussing NAO-related circulation anomalies and downstream-propagating wave trains in the warm and cold ENSO winters. Figure 1 shows the regression of the monthly 300 hPa geopotential height (hereafter Z 300 hPa), SAT anomalies onto the monthly NAO index during the warm and cold ENSO winters. During the warm ENSO winters, a significant ridge with a center over Lake Baikal is found in the high latitudes (40°–65°N) of Asia. The peak amplitude of this ridge is about two-thirds that of the midlatitude lobe of the NAO (see Fig. 1a). Consistent with this ridge, the SAT perturbations associated with the NAO over the high latitudes of Eurasia are also very evident (see Fig. 1c). During the cold ENSO winters, however, over the downstream regions of the NAO, the regressed Z 300 hPa map has three prominent lobes over the Arabian Sea, the east coast of Asia at around 40°N, and the North Pacific (see Fig. 1b), which is very similar to the "NAO-related circumglobal teleconnection" pattern discussed by Branstator (2002, see his Figs. 10 and 16), suggesting that the hemispheric influences of the NAO in cold ENSO winters are related to the Asian jet waveguide. The signatures of the SAT anomalies associated with the NAO over the high latitudes of Eurasia are also relatively weak compared to the warm ENSO winters (see Fig. 1d).

To examine the NAO-related zonally asymmetric teleconnection pattern (wave train), following Watanabe (2004), Fig. 2 shows the circulation anomalies as represented by the 300 hPa meridional wind (hereafter V 300 hPa). For a clear depiction of the different propagation directions of the NAO-related wave trains, corresponding to Plumb (1985), stationary wave-activity fluxes (vectors) during the warm and cold ENSO winters are also shown in Fig. 2. The Plumb stationary wave-activity flux is parallel

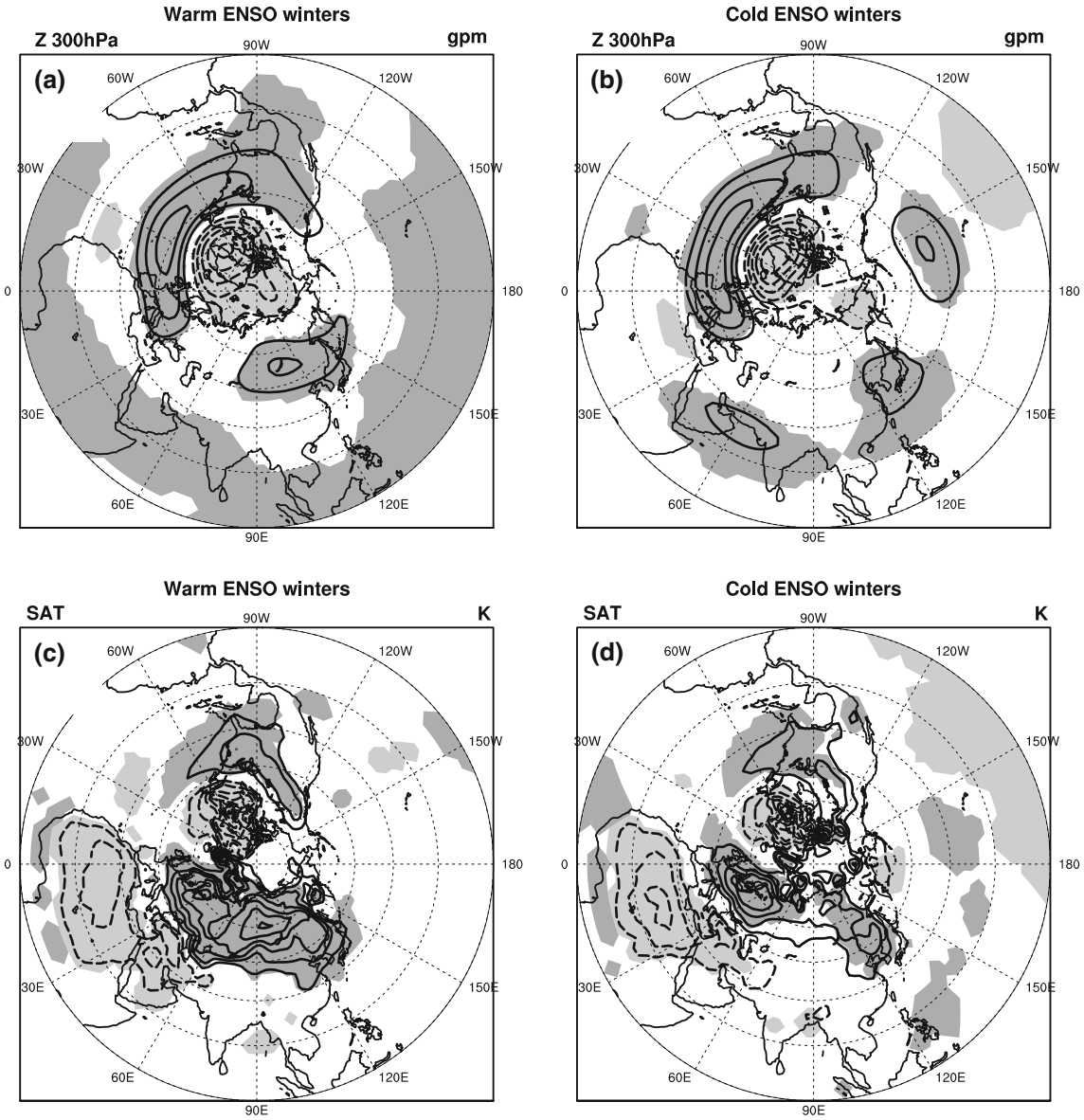

Fig. 1 **a** Monthly anomalous geopotential height at 300 hPa (Z 300 hPa) and **b** near-surface air temperature (SAT) regressed onto the monthly NAO index during the warm ENSO winters (DJF). **c**, **d** As in **a**, **b** but for the regressed results during the cold ENSO winters. *Solid* (*dashed*) *contours* represent positive (negative) values and the zero contours are omitted. The contour interval is 20 gpm for Z 300 hPa and 0.5 K for SAT. The regressed results at the 95 % confidence level are *shaded*

to the local group velocity in the Wentzel–Kramers–Brillouin limit for monochromatic waves and thus approximates the propagation directions for stationary wave trains. From Fig. 2b, it is evident that the NAO-related wave train emanating from the western Atlantic propagates eastward and equatorward from the midlatitudes of the North Atlantic to the subtropical regions of Africa during the cold ENSO winters (Fig. 2b, 40°W–40°E). However, compared to the cold ENSO winters, the structure and propagation direction of the NAO-related wave train during the warm ENSO winters are different (Fig. 2a). The structure of the NAO-related wave train appears to split over Europe. Abatzoglou and Magnusdottir (2004) showed that the observational wave reflection is characterized by a split-wave structure (see their Fig. 2), which is very similar to the split NAO-related wave structure shown in Fig. 2a. We also notice that the wave activity flux directed toward the equator is still observed over the North Atlantic, suggesting that a portion of the NAO-related wave train still has a meridional extension. However, it should be underscored that another portion of the NAO-related wave train abruptly turns to propagate northeastward slightly, extending to the high latitudes of Eurasia (Fig. 2a, 0°–100°E).

Based on the split-wave structure and the very abrupt change in propagation direction, we argue that the NAO-related wave train in warm ENSO winters *might* be interpreted as a nonlinear wave reflection. When the wave propagates from middle and high latitudes to lower latitudes, it is absorbed as it approaches its critical latitude, where the zonal phase speed of the wave matches the background zonal flow. However, if the dissipation is weak or the amplitude of the wave is large, then the wave breaks (McIntyre and Palmer 1983) in the neighborhood of the critical latitude (called the critical layer). According to a theory about the absorption/reflection properties of the critical layer (Killworth and McIntyre 1985), the ability of the critical layer to absorb the momentum flux associated with the incident wave is limited. Therefore, if the amplitude of the incoming wave is large enough, the critical layer may act as a wave reflector (or a wave source) and emit waves toward middle and high latitudes to reduce the net propagation toward it. This process is called nonlinear wave reflection (e.g., Brunet and Haynes 1996; Magnusdottir and Haynes 1999; Walker and Magnusdottir 2003; Abatzoglou and Magnusdottir 2004, 2006a). In Fig. 2, the averaged 300 hPa zonal winds in the warm and cold ENSO winters are also superimposed. Indeed, consistent with the theoretical critical layer argument about the wave reflection, the NAO-related wave train in the warm ENSO winters is reflected (refer to the slightly northeastward-directed wave-activity flux over Eurasia in Fig. 2a) from the latitudes where the zonal wind speed is small and most likely matches the phase speed of the NAO-related wave train.[1]

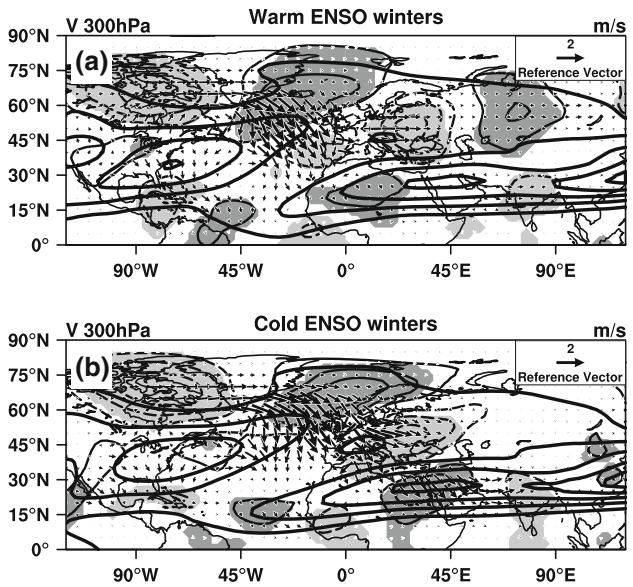

Fig. 2 Regressed monthly anomalous meridional wind at 300 hPa (V 300 hPa, *thin contours*, interval is 1 m/s) onto the monthly NAO index and the corresponding stationary wave activity fluxes (vectors, unit is $m^2\ s^{-2}$) during **a** the warm ENSO winters and **b** cold ENSO winters. *Solid* (*dashed*) *contours* represent positive (negative) values and the zero contours are omitted. The regressed results at the 95 % confidence level are *shaded*. *Thick contours* superimposed in **a** and **b** denote the averaged 300 hPa zonal wind (interval is 10 m/s) in the warm and cold ENSO winters

We consider that the different downstream Z 300 hPa and SAT anomalies associated with the NAO during the warm and cold ENSO winters are related to the very different downstream-propagating directions/pathways of the NAO-related wave train. During the warm ENSO winters, the NAO-related wave train can propagate deeply into the Eurasian continent and produce positive geopotential height/anticyclonic PV anomalies (i.e., the ridge over Lake Baikal) in the upper troposphere over the Asian continent. From the PV thinking (Hoskins et al. 1985), the upper-level positive (negative) PV anomalies can yield warm (cold) temperature anomalies at the ground by pushing (pulling) isentropic surfaces downward (upward) in the troposphere. Therefore, the warm SAT anomalies over Eurasia in the warm ENSO winters are much stronger compared to those in the cold ENSO winters. During the cold ENSO winters, however, supported by a clear sign of the downstream propagation of the wave activity flux along the subtropical Asian jet (Fig. 2b, 40°–80°E), the meridionally propagating NAO-related wave train tends to propagate downstream along the subtropical Asian jet, which is similar to the "Asian jet waveguide-trapped wave train" discussed in Watanabe (2004). Due to the waveguide effect of the subtropical Asian jet, the downstream influence of the NAO is trapped in the subtropical latitudes. Thus, as shown in Fig. 1b, d, the anomalous Z 300 hPa associated with the NAO extends all the way to the North Pacific along the Asian jet waveguide, and the SAT anomalies over the high latitudes of Eurasia are relatively weak.

Table 2 lists the number of positive (NAO index > 0.5), negative (NAO index < -0.5), and neutral ($-0.5 \leq$ NAO index ≤ 0.5) NAO months during the warm and cold ENSO winters. This shows that the distributions of the monthly NAO index in the warm and cold ENSO winters are nearly uniform (the average monthly NAO index in the warm/cold ENSO winters is about $-0.05/0.03$), which, to a large degree, excludes the possibility that the different downstream signatures of the NAO in the warm and cold ENSO winters are attributable to the phase asymmetric downstream development of the NAO (Sung et al. 2010).

The different observed behaviors of the NAO discussed above indicate that the NAO-related wave train has two distinct downstream-propagating directions/pathways.

[1] From the composite results of the life cycle (growth and decay) of the NAO pattern (Feldstein 2003; Jia et al. 2007), the NAO-related wave trains are sufficiently stationary; therefore the phase speed of the NAO-related wave trains should be small.

Table 2 Numbers of positive (NAO index > 0.5), negative (NAO index < −0.5), and neutral (−0.5 ≤ NAO index ≤ 0.5) NAO months during the warm and cold ENSO winters

	NAOI > 0.5	NAOI < −0.5	−0.5 ≤ NAOI ≤ 0.5
Warm ENSO winters	20	21	16
Cold ENSO winters	20	17	26
Other winters	65	56	62

Accordingly, the downstream circulation and SAT anomalies associated with the NAO are also very different. Based on these results, and as mentioned in the introduction, we argue that the downstream influence of the NAO is of two distinct types: the H type (Fig. 2a) and the L type (Fig. 2b).

3.2 Ratios of the *H* and *L* types of NAO

In this subsection, the ratios of the *H* and *L* types of NAO in both phases of the strong NAO days are roughly evaluated and discussed. It is noticed that the most conspicuous difference between the *L* and *H* types of NAO is the different meridional propagation directions of the NAO-related downstream wave trains. The *L* (*H*) type of NAO-related downstream wave train corresponds primarily to a southward (northward) propagation over Europe (see Fig. 2). Therefore, we might use the averaged meridional component of the wave activity flux over Europe to identify the *L* or *H* type of NAO. To do that, first, the strong positive and negative NAO days are extracted based on one standard deviation of the normalized daily NAO index. Then, based on the total circulation anomalies on those strong NAO days, the Plumb stationary wave activity flux is calculated to indicate the propagation direction of the NAO-related downstream wave train. For each strong NAO day, the corresponding Plumb wave activity flux is averaged over a box region (40°–60°N, 0°–60°E), which roughly represents the continent of Europe. If the averaged meridional component of the wave activity flux is poleward (equatorward)-directed, then the downstream influence of the NAO is defined to be the *H*(*L*) type.

In the 5,490 days of data, there are 876 positive strong NAO days (NAO index ≥ 1.0) and 920 negative strong NAO days (NAO index ≤ −1.0) in all. Based on the procedure that we described above, there are 158 (18.0 %) of the *H* type and 718 of the *L* type in the positive strong NAO days. For the negative strong NAO days, the number of the *H* type is 289 (31.4 %) and the number of the *L* type is 631. For all strong NAO days (positive and negative), the percentage of the *H* type is about 25 %. It is clear that the percentage of the *H* type for the negative strong NAO days is about two times greater than that for the positive strong NAO days. This might be due to the negative NAO arising from cyclonic wave breaking (Benedict et al. 2004), which corresponds to very weak meridional radiation (Thorncroft et al. 1993). Thus, more negative NAO days tend to be identified as the *H* type. In addition, Abatzoglou and Magnusdottir (2006a) have showed that, for the reflective waves, the PV meridional gradient immediately northeast of the wave-breaking region should be strong enough to support the propagation of the reflected wave train out of the wave-breaking region. Composite PV fields on the 320 K isentropic surface (using ERA-40 daily data) for the strong positive and negative NAO indicate that the PV meridional gradient immediately northeast of the wave-breaking region for the positive NAO is weaker compared to the negative NAO (not shown). Thus, the background flow does not favor the propagation of the reflective wave train out of the wave-breaking region, resulting in less of the *H* type being identified for the positive NAO. Certainly, we cannot rule out the possibility that other factors also contribute to the lower percentage of the *H* type in the positive strong NAO days, such as the latitudinal positions of synoptic-scale waves associated with the NAO. Franzke et al. (2004) argued that the synoptic waves that precede the formation of the positive (negative) NAO tend to occur on the equatorward (poleward) side of the midlatitude jet. Thus, the synoptic waves undergo anticyclonic (cyclonic) shears in the positive (negative) NAO, which favors the presence of equatorward (poleward) wave activity flux. Thus, the *H* type is less (more) frequently detected for the positive (negative) strong NAO.

It should be noted that the evaluation of the ratios of the *H* and *L* types of NAO is very rough, since the only criterion for this classification is the averaged meridional component of the Plumb wave activity flux over a box region (40°–60°N, 0°–60°E). The wave activity flux is calculated based on the *total* circulation anomalies, which certainly cannot be completely explained by variations in the NAO. Therefore, strictly speaking, an averaged poleward (equatorward)-directed wave activity flux over the downstream regions of the NAO does not definitely guarantee that each strong NAO that we identify is "indeed" the *H*(*L*) type. Fortunately, this uncertainty can be largely eliminated by using composite analysis. The composite Z 300 hPa and V 300 hPa anomalies for the *H*/*L* types of positive and negative NAO are shown in Figs. 3 and 4. It is found that the downstream circulation anomalies and wave trains associated with the *H* and *L* types NAO that we define are indeed different. Especially, over the high latitudes of East Asia, there is a ridge (trough) corresponds to the *H* type positive (negative) NAO (see Figs. 3a, 4a). However, in the same area, the ridge/trough becomes much weaker for the *L* type NAO. Actually, the *L* type NAO is

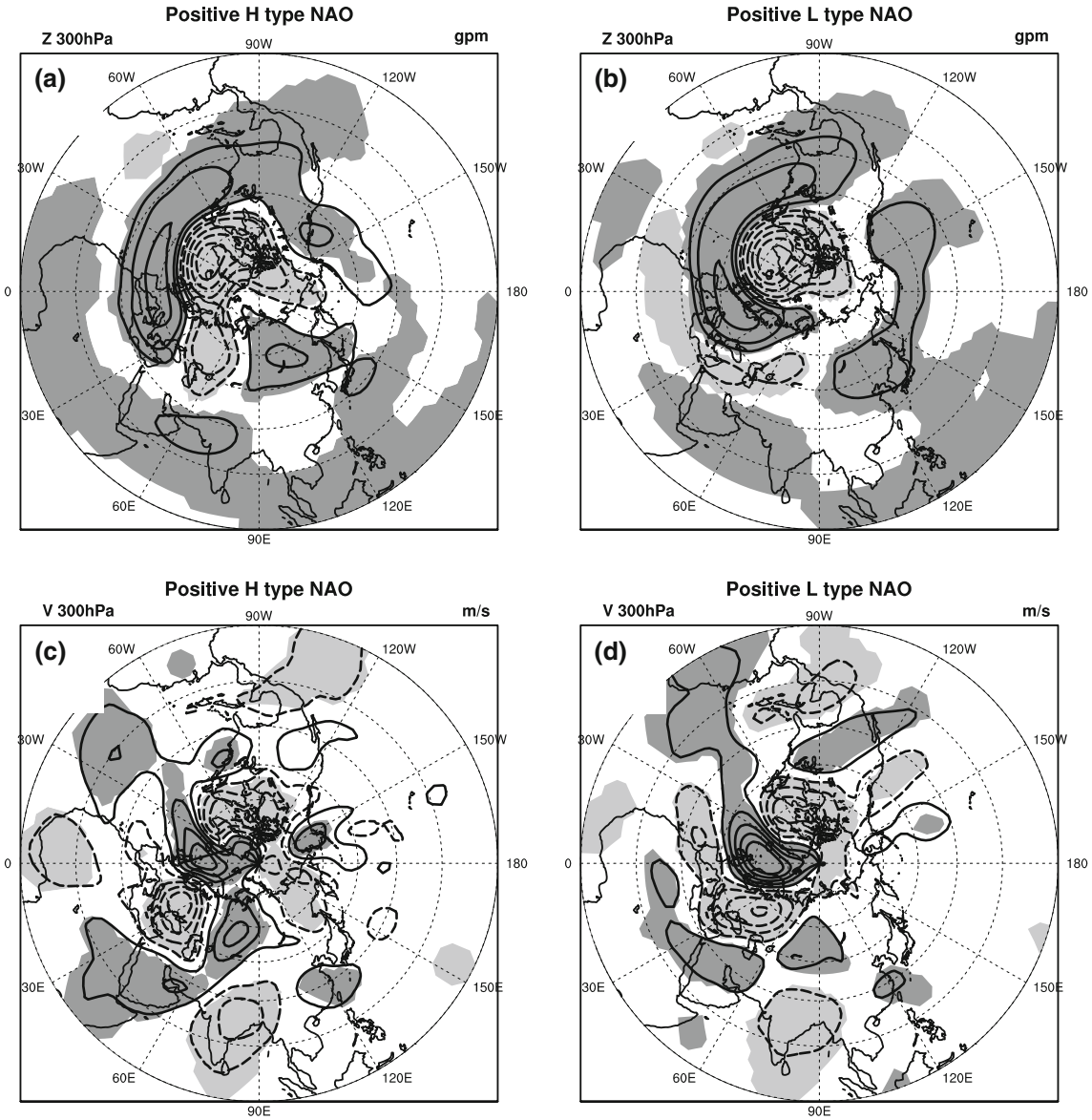

Fig. 3 Composites of 300 hPa geopotential height (Z 300 hPa) anomalies for the positive **a** *H* type of NAO and **b** *L* type of NAO. **c**, **d** As in **a**, **b** but for composites of 300 hPa meridional wind (V 300 hPa) anomalies. *Solid* (*dashed*) *contours* represent positive (negative) values and the *zero contours* are omitted. Contours are drawn at intervals of (±20, ±50, ±100, ±150, …) for *Z* 300 hPa and (±1, ±3, ±5, ±7, …) for V 300 hPa. The composite results at the 95 % confidence level are *shaded*

associated with significant Z 300 hPa anomalies over the Arabian Sea, the east coast of Asia at around 40°N, and the North Pacific (see Figs. 3b, 4b). Observed from the composite V 300 hPa anomalies, there is a zonally downstream extending wave train over the high latitudes of Eurasia for the *H* type NAO (see Figs. 3c, 4c); while it is less evident in the composite result of the *L* type NAO (see Figs. 3d, 4d). The *L* type NAO is associated with a wave train that primarily propagates in a meridional direction from the North Atlantic to the subtropical regions of Africa/Middle East (see Figs. 3d, 4d). We also notice that the split-wave structure for the *H* type NAO (see Fig. 4c) and a wave train downstream propagating along a subtropical path for the *L* type NAO (see Fig. 4d) are evident in the negative NAO composite V 300 hPa anomalies. However, these features are hardly observed in the *H* and *L* types positive NAO composites (see Fig. 3c, d). This might be due to our rough identify method for the *H* and *L* types NAO. Generally speaking, from these composite results, we conclude that their circulation anomalies and wave train propagation directions are similar to those based on ENSO. Therefore, although the detection of the H and L types of NAO is rough, the ratios of the *H* and *L* types of NAO presented here are still meaningful. To confirm that these ratios are

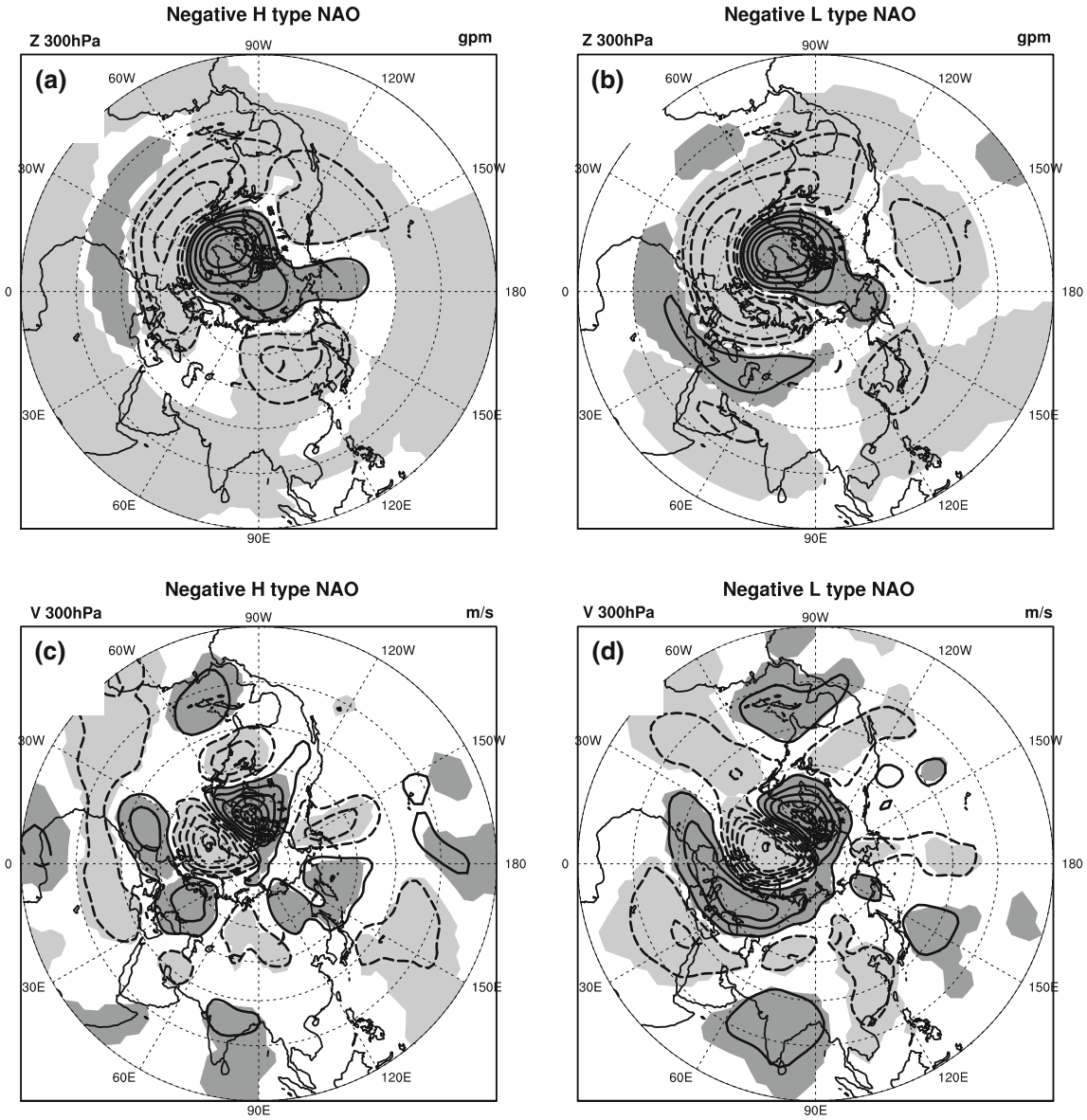

Fig. 4 As in Fig. 3 but for the negative *H* and *L* types of NAO

robust, we also slightly change the domain of the box region for averaging the meridional wave-activity flux, and we find that the ratios of the *H* and *L* types for the positive and negative NAO are qualitatively unchanged, although the number of *H* and *L* types of NAO varies slightly.

3.3 Possible role of the subtropical PV meridional gradient

Why do the types of NAO's downstream influence (or the propagation directions/pathways of the NAO-related downstream wave train) differ during the warm and cold ENSO winters? We argue that the different intensities of the subtropical PV meridional gradient over Africa might be an important factor responsible for this. Figure 5 shows the composite PV meridional gradient anomalies on the 320 K isentropical surface (320 K PV gradient hereafter) during the warm and cold ENSO winters. The climatological 320 K PV gradient in boreal winters is also superimposed. The intensity of the PV gradient over subtropical Africa is weaker (stronger) during the warm (cold) ENSO winters. It is known that the background PV meridional gradient plays an important role in determining whether the waves undergo reflection or nonreflection. That is, a stronger (weaker) PV meridional gradient tends to hamper (facilitate) the wave's reflection (e.g., Abatzoglou and Magnusdottir 2006a). Therefore, it is plausible that in the warm ENSO winters, due to the weaker

subtropical PV gradient over Africa, the NAO-related downstream-propagating wave train has a greater possibility of being reflected back to high latitudes before it can disturb the circulations over the entrance of the Asian jet. So the "Asian jet waveguide-trapped wave train" is rarely excited, and the NAO's downstream influence tends to be of the *H* type. For the cold ENSO winters, however, the NAO-related wave train can easily impact the circulations over the entrance of the Asian jet, exciting the quasi-stationary waves propagating downstream along the subtropical Asian jet waveguide, since a stronger subtropical PV gradient over Africa is less capable of reflecting the wave train back. Therefore, the NAO's downstream influence tends to be of the *L* type. *We consider that whether the NAO-related downstream-propagating wave train undergoes reflection or nonreflection may be fundamental in determining the so-called H or L type of NAO's downstream influence.*

Figure 6 shows the composite of the 320 K PV gradients for the H type of NAO (positive and negative phases) that we selected in Sect. 3.2. To highlight the characteristics of the PV gradient of the *H* type of NAO, the differences in the composite of the 320 K PV gradient between the *H* type of positive (negative) NAO and all the strong positive (negative) NAO days are also superimposed in Fig. 6. It is evident that for the H type of NAO (whether positive or negative), the PV gradient is weaker around 40°N over the African sector. Thus, although with a northward displacement, these results partly support our argument that the types of NAO's downstream influence are related to the intensities of the subtropical PV gradient over Africa.[2] In addition, we also note that the PV gradients are stronger to the north of subtropical Africa, which is also observed in Fig. 5a. These stronger PV gradients are consistent with the poleward-directed wave activity flux over Europe for the detection of the *H* type NAO. When the wave tends to propagate poleward, then the anomalous eddy PV flux associated with the wave deposits to its south increasing the PV gradient (Vallis 2006). These stronger PV meridional gradients also consistent with the results of Abatzoglou and Magnusdottir (2006a), who found that compared to the nonreflective wave, the PV meridional gradients immediately northeast of the reflective wave-breaking region are stronger and so can support the

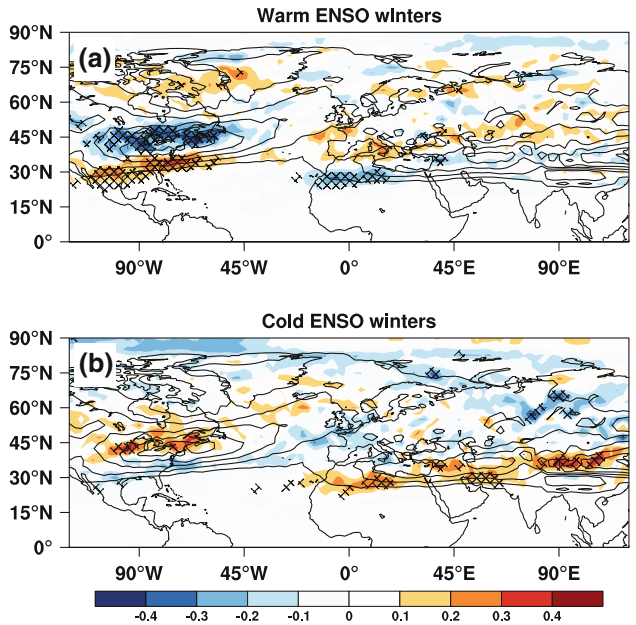

Fig. 5 Composite 320 K PV gradient anomalies (*shaded*, unit is 1.0×10^{-6} PVU/m, 1 PVU $= 1.0 \times 10^{-6}$m^2 s^{-1} K kg^{-1}) during **a** the warm and **b** cold ENSO winters. The composite results at the 95 % confidence level are hatched. The climatological 320 K PV gradient in boreal winters is also superimposed (contours, interval is 0.5×10^{-6} PVU/m)

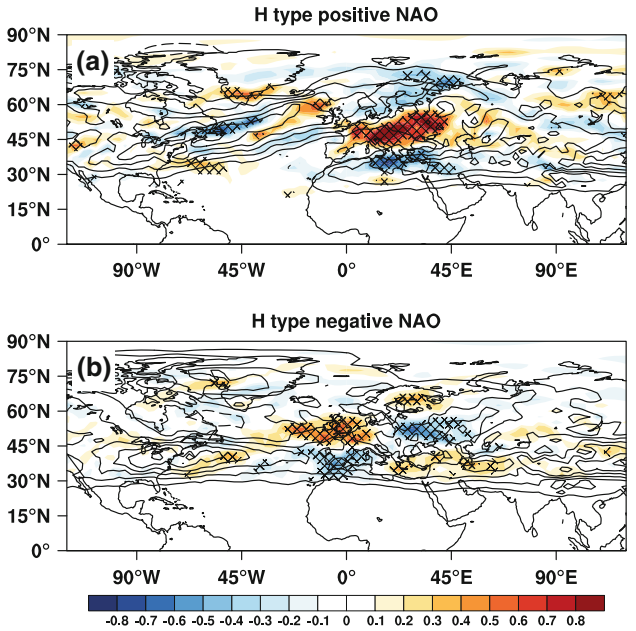

Fig. 6 Meridional gradients (contours, interval is 0.5×10^{-6} PVU/m, 1 PVU $= 1.0 \times 10^{-6}$m^2 s^{-1}K kg^{-1}) of the composite of 320 K PV for **a** the *H* type of positive NAO and **b** *H* type of negative NAO. *Shaded areas* (unit is 1.0×10^{-6} PVU/m) denote their differences with the meridional gradients of the composite of 320 K PV for all strong positive and negative NAO, respectively. The differences at the 95 % confidence level are hatched

[2] This somehow northward displacement of the weaker PV gradient might be due to our rough method for detection of the *H* and *L* type daily NAO. We also detection the *H* and *L* type NAO winters. In this detection, the NAO-related circulation anomalies for the calculation of wave flux are acquired by regressing the daily data onto the daily NAO index, which can be considered as "indeed the anomalous circulation associated with the NAO". In this analysis, we find that, in the *H* type NAO winters, the intensity of the background subtropical African jet is weaker and well consistent with the results shown in Fig. 5 (not shown).

propagation of the reflected wave train out of the wave-breaking region.

The above discussion indicates that the intensity of the subtropical PV gradient over Africa may play a role in modulating the types of NAO's downstream influence. To further support this argument, winters with a strong and weak background subtropical PV gradient are selected based on a subtropical PV gradient intensity index. This index is acquired by averaging the winter 320 K PV gradient over a subtropical box region (20°–30°N, 20°W–40°E). The monthly NAO index regressed V 300 hPa anomalies and corresponding Plumb stationary wave-activity fluxes in those strong and weak subtropical PV winters are shown in Fig. 7. The results are similar to the results of the cold and warm ENSO winters (see Fig. 2). The NAO-related wave train propagates downstream primarily along a low (high)-latitude pathway in the strong (weak) PV gradient winters. These results indicate that the NAO's downstream influence is apt to be of the H(L) type during weak (strong) PV gradient winters, which confirms our argument that the intensity of the subtropical PV gradient over Africa might plays a role in modulating the types of NAO's downstream influence.

3.4 Intraseasonal NAO events

Although the NAO is known to be a dominant pattern in atmospheric variability in the North Atlantic on multiple time scales, many studies concerning the origin of the NAO have indicated that the fundamental dynamic processes of the NAO lie in intraseasonal time scales (e.g., Benedict et al. 2004; Rivière and Orlanski 2007; Luo et al. 2007), namely, the growth and decay of NAO events (Feldstein 2003). In this subsection, we extend our analysis to the short life cycles of positive and negative NAO events by using daily data.

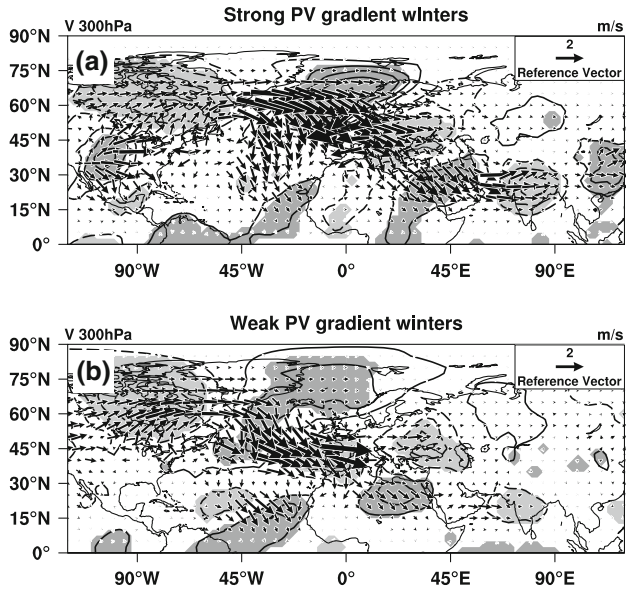

Fig. 7 Regressed monthly anomalous meridional wind at 300 hPa (V 300 hPa, thin contours, interval is 1 m/s) onto the monthly NAO index and the corresponding stationary wave activity fluxes (vectors, unit is $m^2\ s^{-2}$) during **a** the strong subtropical PV gradient winters and **b** weak subtropical PV gradient winters. *Solid* (*dashed*) *contours* represent positive (negative) values and the zero contours are omitted

We aim to answer two questions: (1) Can the H and L types of NAO-related downstream wave train be identified in intraseasonal NAO events? (2) As we argued in Sect. 3.3, the PV gradient of subtropical Africa plays an important role in modulating the propagation direction of the NAO-related wave train. Can this argument be verified in intraseasonal NAO events? To answer these questions, we first identify every intraseasonal positive/negative NAO event from the 45 boreal winters covered by the ERA-40 daily data. Second, these positive/negative NAO events are separated into two categories in terms of an intensity threshold of the PV gradient over subtropical Africa. Third, we compare composites of these two categories of positive/negative NAO event life cycles. If our argument is correct, then the two sets of positive/negative NAO event composites should be conspicuously different: the NAO-related wave train in the one with sharp (gentle) subtropical PV gradients will propagate downstream along a low (high)-latitude path.

NAO events are defined based on the daily NAO index. Since the decorrelation time of the daily NAO index is about 6 days (Watanabe 2004), our method of identifying NAO events is straightforward. First, strong positive and negative NAO days are selected based on one standard deviation of the normalized daily NAO index. For each strong positive (negative) NAO day, if the NAO index of that day is higher (lower) than on any of the 6 days preceding or following it (lag −6 to +6 day), then that day is defined as the peak or mature day (0 day) of a positive (negative) NAO event. The period of time from lag −6 to +6 day is defined as a positive (negative) NAO event. To ensure that the identified NAO events are independent from each other, the peak day of each NAO event must be separated by at least 10 days. Based on this procedure, 103 positive and 86 negative NAO events are identified from the ERA-40 daily data. Consistent with Watanabe (2004), it is found that there are slightly more positive events than negative events, despite the different procedure for detecting NAO events. Our composite results are not sensitive to our method of defining NAO events: when we repeated the analysis and used the method of Watanabe (2004) to detect NAO events, the results were qualitatively unchanged.

For individual positive NAO events, a subtropical PV gradient intensity index is acquired by averaging the 320 K PV gradients over a box region (20°–30°N, 20°W–40°E)

from lag 0 to +6 day to represent the intensity of the PV gradient of subtropical Africa. We normalize the time series of the PV gradient intensity index. Then, taking 0.5 standard deviation of that index as a threshold, 33 (34) positive NAO events accompanied by sharp (gentle) PV gradients are selected from the 103 positive NAO events. Similar procedures are applied to the 86 negative NAO events; we obtain 29 (30) negative NAO events accompanied by sharp (gentle) PV gradients. However, for the negative NAO events, the box region for averaging the PV gradients is shifted 10° to the north (30°–40°N, 20°W–40°E), because the high PV gradient band over subtropical Africa shifts northward more during negative NAO events than during positive NAO events. Therefore, for negative NAO events, a corresponding northward shift of the box region will better represent the intensity of the PV gradient over subtropical Africa.

The composite time evolution of the positive (negative) NAO events accompanied by sharp and gentle subtropical PV gradients in terms of 300 hPa 10-day lowpass meridional wind anomalies from lag 0 to lag +6 days is illustrated in Fig. 8 (Fig. 9). Generally, in the NAO composite anomalies that accompany sharp subtropical PV gradients (whether in the positive or negative phase), the NAO-related wave train first propagates in the meridional direction (lag 0 to +2 day). Then, after 2 days, a wave train pattern propagating downstream along the Asian jet is observed (lag +4 to +6 day). This wave train pattern is very similar to the waveguide pattern discussed by Watanabe (2004, see his Fig. 13). On the other hand, in the anomalies with gentle subtropical PV gradients, we observe a split wave pattern that suggests the wave is reflected from lag 0 to +2 day. Subsequently, an eastward-propagating wave train along a high-latitude path is observed (lag +4 to +6 day).

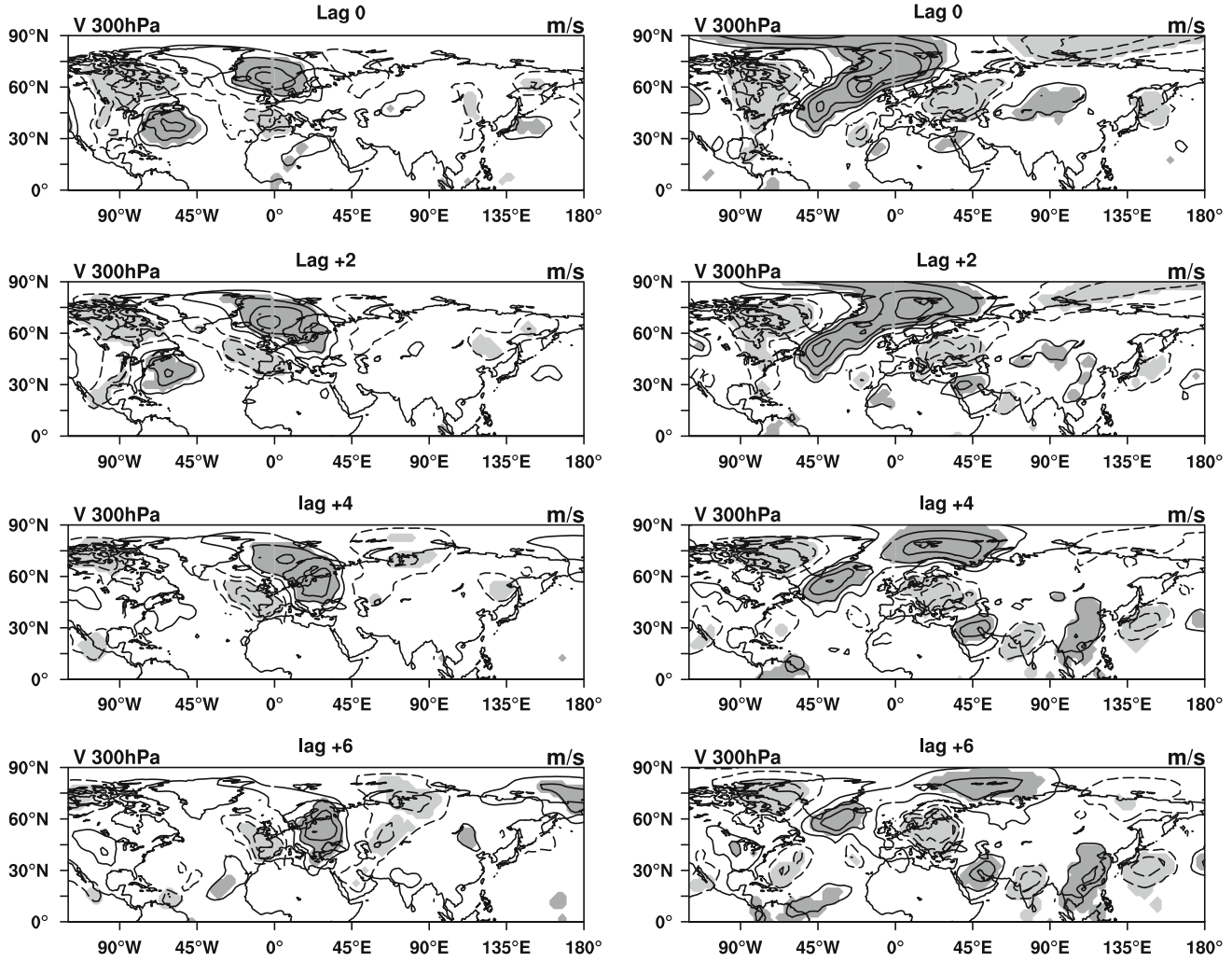

Fig. 8 Composite anomalies of 300 hPa meridional wind for the positive phase of the NAO events that accompany a weak (*left column*) and sharp (*right column*) PV gradient over subtropical Africa. Lag 0 corresponds to the peak day, while lag +2, +4, and +6 correspond to the subsequent anomalies at days 2, 4, and 6, respectively. The contour interval is 2 m/s. *Solid* (*dashed*) *contours* represent positive (negative) values and the zero contours are omitted. The composite results at the 95 % confidence level are *shaded*

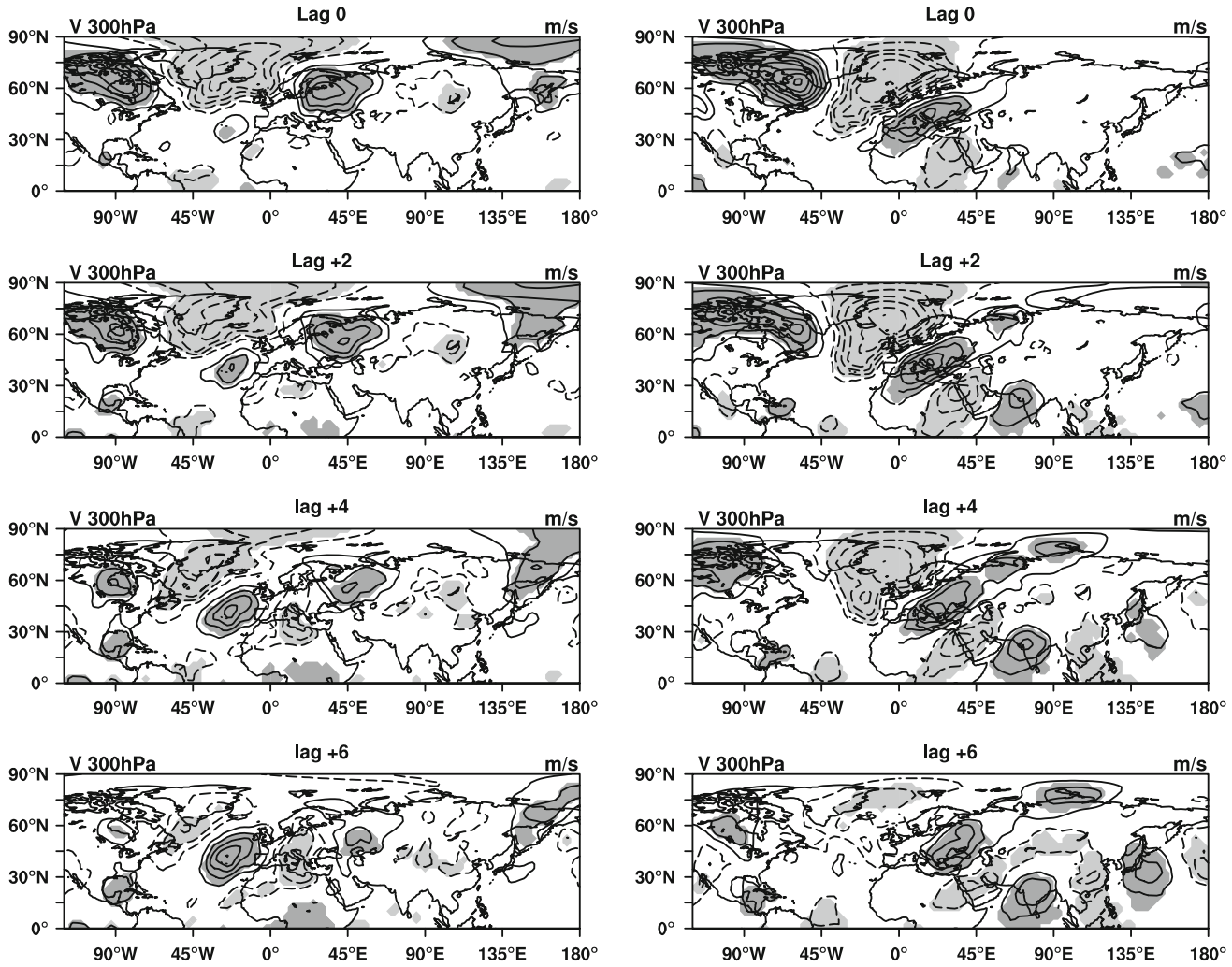

Fig. 9 As in Fig. 8 but for the negative phase of the NAO events

Clearly, the composite time evolutions of the intraseasonal NAO events with strong and gentle PV gradients over subtropical Africa support our main conclusions. The existence of the H and L types of NAO-related downstream wave train is evident even in intraseasonal NAO events. The propagation directions/pathways of the NAO-related downstream wave train are modulated by the intensity of the PV gradient over subtropical Africa.

4 Summary and discussion

4.1 Summary

This study uses reanalysis data to investigate the different types of downstream influence of the NAO. It is found that the NAO's influence as well as the propagation direction of the NAO-related wave train during the warm and cold ENSO boreal winters is significantly different. During the cold ENSO winters, the NAO-related wave train propagates downstream primarily along a low-latitude pathway, which is similar to the "Asian jet waveguide-trapped Rossby wave" in Watanabe (2004). During the warm ENSO winters, the NAO-related wave train propagates downstream primarily along a high-latitude pathway, which might be interpreted as nonlinear wave reflection. During the cold ENSO winters, the NAO is associated with significant Z 300 hPa anomalies over the Arabian Sea, the east coast of Asia at around 40°N, and the North Pacific, which is very similar to the "NAO-related circumglobal teleconnection" pattern discussed by Branstator (2002), whereas during the warm ENSO winters, there is a ridge associated with the NAO over the high latitudes of Asia. Consistent with the NAO-related Z 300 hPa anomalies, the NAO-related SAT anomalies over the high latitudes of Eurasia are also relatively weak (strong) in the cold (warm) ENSO winters. Based on these different behaviors of the NAO during the cold and warm ENSO winters, we argue

that the NAO has two distinct types of downstream influence: the L (low-latitude) and H (high-latitude) types. The ratios of the L and H types in both phases of strong NAO days are also roughly evaluated using daily data. The poleward/equatorward average meridional component of wave activity flux over Europe is used to identify the H or L type of NAO. We find that the percentage of the H type for negative strong NAO days (31.4 %) is about two times greater than that for positive strong NAO days (18.0 %).

We consider that whether the NAO-related downstream-propagating wave undergoes reflection or nonreflection is the fundamental factor responsible for the so-called H or L type of NAO downstream influence. Since a stronger (weaker) PV meridional gradient tends to hamper (facilitate) the reflection of the wave, we therefore argue, based on the wave reflection/nonreflection idea, that the intensity of the PV gradient over subtropical Africa plays a role in modulating the propagation directions of the NAO-related wave train and thus the types of NAO's downstream influence. In other words, the downstream-propagating NAO-related wave train tends to be of the L (H) type when the subtropical PV gradient over Africa is strong (weak). This argument is validated by the NAO regressed V 300 hPa anomalies in the winters accompanied by strong and weak background subtropical PV gradients over Africa. Consistent with this argument, the composite results of the PV gradient of the H type NAO days that we selected show that the PV meridional gradient around 40°N over the African sector is anomalously weak.

The existence of the two types of NAO-related wave train and the modulating effect of the subtropical PV gradient are also evident in our analysis of intraseasonal NAO events. Using daily data, the short life cycles of positive and negative NAO events are identified. We separate these NAO events into two categories in terms of the intensity of the PV gradient over subtropical Africa. The composite time evolution of the NAO events with a weak (strong) subtropical PV gradient clearly shows that the NAO-related wave train tends to propagate along a high (low)-latitude pathway.

4.2 Discussion

Traditionally, the NAO has been recognized as a regional mode of variability over the Euro-Atlantic region. The pioneering work of Branstator (2002) and Watanabe (2004) presented the "Asian jet waveguide-trapped wave train" mechanism to understand the downstream influence of the NAO, in particular, the SAT perturbation associated with the NAO over Asia. However, their studies emphasized the waveguide effect of the subtropical Asian jet and revealed only the low-latitude pathway of the NAO's downstream influence. The high-latitude pathway of the NAO's downstream influence presented in this study complements the "Asian jet waveguide-trapped wave train" mechanism.

Abatzoglou and Magnusdottir (2006b) discussed the different effects of reflective and nonreflective anticyclonic planetary wave breaking on the NAO. They found that the positive phase of the NAO is formed when there is anticyclonic planetary wave breaking over the North Atlantic. The positive NAO tends to amplify and persist when the breaking wave is nonreflective, whereas if the breaking wave is reflective, the signal of the positive NAO declines quickly and the polarity of the NAO is reversed. They also found a poleward-arching wave pattern over Eurasia after the reflective wave breaking (see their Fig. 3a). Thus, it seems that the H type of NAO's downstream influence presented in this study overlaps with the findings of Abatzoglou and Magnusdottir (2006b). However, we must point out that the "poleward-arching wave train" in the reflective cases discussed by Abatzoglou and Magnusdottir (2006b) is in fact a meridional propagation wave train (similar to our Fig. 2b). They describe this wave train as being "evident 2 days following the break, a clear signal is seen extending well over Europe and into the Middle East" (see also their Fig. 3a). Clearly, this wave train is completely different from our "poleward-arching wave train," which propagates into the high latitudes of Eurasia (see Fig. 2a).

Due to the distinct effects of the L and H types of NAO's downstream influence, the linkages between the NAO and climate variability in East Asia are different. For example, Wang et al. (2010) suggested that the variability of the East Asian winter monsoon (EAWM) is dominated by two distinct SAT modes: the northern temperature mode and the southern temperature mode. We find that the spatial distribution of NAO-related SAT anomalies in the H type is similar to that of the SAT anomalies associated with the northern temperature mode of the EAWM. Therefore, we expect the close degree of linkage between the NAO and the northern temperature mode of the EAWM to be remarkably improved with the H type of NAO's downstream influence. This is true; the NAO's downstream influence tends to be of the H(L) type during the warm (cold) ENSO winters, and the correlation coefficient between the NAO index and the northern temperature mode index during these winters is 0.660 (0.387).

In the DJF of 2009/10, the Niño 3 SST anomaly averaged about 1 Celsius degree, indicating an El Niño event of notable intensity. The NAO index for December 2009–February 2010 was −2.52 standard deviations (making this a highly unusual event; NOAA Attribution Team 2010; Ouzeau et al. 2011). This very cold winter in the NH is thought to be due to the extreme negative NAO during this time. The spatial patterns of the monthly Z 300 hPa, SAT, and V 300 hPa anomalies from December 2009 to

February 2010 (not shown) indicate that the circulation anomalies in the middle to high latitudes of the NH are in excellent agreement with the H type of NAO's downstream influence discussed in this study. Therefore, we consider that this winter provides a good example of the H type NAO and its unique downstream influence.

Acknowledgments The authors would like to thank three anonymous reviewers and editor Edwin K. Schneider for their helpful comments that led to the substantial improvement of this paper. This work is sponsored by the Key Technologies R&D Program (Grant No. 2009BAC51B02) and National Nature Science Foundation of China (Grant No. 41275086 and 40805023). The work is also partially supported by a grant from the Research Grants Council of the Hong Kong Special Administrative Region (Project No. 104410). JS and CYL are supported by the 973 program (Grant No. 2010CB950401) and National Nature Science Foundation of China (Grant No. U0833602). JS is also supported by the LASG Free Exploration Fund.

References

Abatzoglou JT, Magnusdottir G (2004) Nonlinear planetary wave reflection in the troposphere. Geophys Res Lett 31:L09101

Abatzoglou JT, Magnusdottir G (2006a) Planetary wave breaking and nonlinear reflection: seasonal cycle and interannual variability. J Clim 19:6139–6152

Abatzoglou JT, Magnusdottir G (2006b) Opposing effects of reflective and nonreflective planetary wave breaking on the NAO. J Atmos Sci 63:3448–3457

Barnston AG, Livezey RE (1987) Classification, seasonality and persistence of low-frequency atmospheric circulation patterns. Mon Wea Rev 115:1083–1126

Benedict J, Lee S, Feldstein SB (2004) Synoptic view of the North Atlantic Oscillation. J Atmos Sci 61:121–144

Branstator G (2002) Circumglobal teleconnections, the jet stream waveguide, and the North Atlantic Oscillation. J Clim 15:1893–1910

Brönnimann S et al (2007) ENSO influence on Europe during the last centuries. Clim Dyn 28:181–197

Brunet G, Haynes PH (1996) Low-latitude reflection of Rossby wave trains. J Atmos Sci 53:482–496

Chang EKM, Yu DB (1999) Characteristics of wave packets in the upper troposphere. Part I: northern Hemisphere winter. J Atmos Sci 56:1708–1728

Feldstein SB (2003) The dynamics of NAO teleconnection pattern growth and decay. Q J Roy Meteorol Soc 129:901–924

Franzke C, Lee S, Feldstein SB (2004) Is the North Atlantic Oscillation a breaking wave? J Atmos Sci 61:145–160

Gouirand I, Moron V (2003) Variability of the impact of El Niño-Southern oscillation on sea-level pressure anomalies over the North Atlantic in January to March (1874–1996). Int J Climatol 23:1549–1566

Gouirand I, Moron V, Zorita E (2007) Teleconnections between ENSO and North Atlantic in an ECHO-G simulation of the 1000–1990 period. Geophys Res Lett 34:L06705

Greatbatch RJ (2000) The North Atlantic Oscillation. Stochastic environemental research and risk assessment. http://www.physoz.icbm.de/download/cl_dyn/full/nao/NAO.pdf

Hoskins BJ, Ambrizzi T (1993) Rossby wave propagation on a realistic longitudinally varying flow. J Atmos Sci 50:1661–1671

Hoskins BJ, McIntyre ME, Robertson AW (1985) On the use and significance of isentropic potential vorticity maps. Q J Roy Meteorol Soc 111:877–946

Hurrell JW (1995) Decadal trends in the North Atlantic Oscillation: regional temperatures and precipitation. Science 269:676–679

Hurrell JW (1996) Influence of variations in extratropical wintertime teleconnections on Northern Hemisphere temperature. Geophys Res Lett 23:665–668

Hurrell JW, Van Loon H (1997) Decadal variations in climate associated with the North Atlantic Oscillation. Climatic Change 36:301–326

Hurrell JW, Kushnir Y, Ottersen G, Visbeck M (2003) An overview of the North Atlantic Oscillation. In: Hurrell JW et al (ed) The North Atlantic Oscillation: climatic significance and environmental impact. Geophys Monogr Ser 134:1–35

Jia X, Derome J, Lin H (2007) Comparison of the life cycles of the NAO using different definitions. J Clim 20:5992–6011

Kalnay E et al (1996) The NCEP/NCAR 40-year reanalysis project. Bull Am Meteor Soc 77:437–470

Killworth PD, McIntyre ME (1985) Do Rossby-wave critical layers absorb, reflect or over-reflect? J Fluid Mech 161:449–492

Lee S (2000) Barotropic effects on atmospheric storm tracks. J Atmos Sci 57:1420–1435

Li Y, Lau NC (2012) Impact of ENSO on the Atmospheric Variability over the North Atlantic in late winter: role of transient eddies. J Clim 25:320–342

Li J, Yu R, Zhou T (2008) Teleconnection between NAO and climate downstream of the Tibetan Plateau. J Clim 21:4680–4690

Luo D, Lupo AR, Wan H (2007) Dynamics of eddy-driven low-frequency dipole modes. Part I: a simple model of North Atlantic Oscillations. J Atmos Sci 64:3–28

Magnusdottir G, Haynes P (1999) Reflection of planetary waves in three-dimensional tropospheric flows. J Atmos Sci 56:652–670

Marshall J et al (2001) North Atlantic climate variability: Phenomena, impacts and mechanisms. Int J Climatol 21:1863–1898

McIntyre ME, Palmer TN (1983) Breaking planetary waves in the stratosphere. Nature 305:593–600

Melo-Goncalves P et al (2005) North Atlantic Oscillation sensitivity to the El Niño/Southern Oscillation polarity in a large-ensemble simulation. Clim Dyn 24:599–606

Moron V, Plaut G (2003) The impact of El Niño-Southern Oscillation upon weather regimes over Europe and the North Atlantic during boreal winter. Int J Climatol 23:363–379

Müller WA, Roeckner E (2006) ENSO impact on midlatitude circulation patterns in future climate change projections. Geophys Res Lett 33:L05711

Ouzeau G et al (2011) European cold winter 2009–2010: how unusual in the instrumental record and how reproducible in the ARPEGE-climate model? Geophys Res Lett 38:L11706

Plumb RA (1985) On the three-dimensional propagation of stationary waves. J Atmos Sci 42:217–229

Pozo-Vázquez D et al (2001) The association between ENSO and winter atmospheric circulation and temperature in the North Atlantic Region. J Clim 14:3408–3420

Rivière G, Orlanski I (2007) Characteristics of the Atlantic storm-track eddy activity and its relation with the North Atlantic Oscillation. J Atmos Sci 64:241–266

Song J, Zhou W, Wang X, Li CY (2011) Zonal asymmetry of the annular mode and its downstream subtropical jet: an idealized model study. J Atmos Sci 68:1946–1973

Sung MK, Lim GH, Kug JS (2010) Phase asymmetric downstream development of the North Atlantic Oscillation and its impact on the East Asian winter monsoon. J Geophys Res 115:D09105

NOAA Attribution Team (2010) Understanding the Mid-Atlantic Snowstorms During the Winter of 2009–2010. Publishing NOAA website. http://www.esrl.noaa.gov/psd/csi/images/NOAA_AttributionTeam_SnowstormReport.pdf. Accessed 27 Sep 2011

Thorncroft CD, Hoskins BJ, McIntyre ME (1993) Two paradigms of baroclinic-wave life-cycle behavior. Q J Roy Meteorol Soc 119:17–55

Trenberth KE et al (1998) Progress during TOGA in understanding and modeling global teleconnections associated with tropical sea surface temperatures. J Geophys Res 103:14291–14324

Trigo RM, Osborn TJ, Corte-Real JM (2002) The North Atlantic Oscillation influence on Europe: climate impacts and associated physical mechanisms. Clim Res 20:9–17

Uppala SM et al (2005) The ERA-40 reanalysis. Q J Roy Meteorol Soc 131:2961–3012

Vallis GK (2006) Atmospheric and Oceanic fluid dynamics. Cambridge University Press, Cambridge

Van Loon H, Rogers JC (1978) The seesaw in winter temperature between Greenland and northern Europe. Part I: general description. Mon Wea Rev 106:296–310

Walker CC, Magnusdottir G (2003) Nonlinear planetary wave reflection in an atmospheric GCM. J Atmos Sci 60:279–286

Wang B et al (2010) Another look at interannual-to-interdecadal variations of the East Asian winter monsoon: the Northern and Southern temperature modes. J Clim 23:1495–1512

Watanabe M (2004) Asian jet waveguide and a downstream of the North Atlantic Oscillation. J Clim 17:4674–4691

Wettstein J, Wallace JM (2010) Observed patterns of month-to-month storm-track variability and their relationship to the background flow. J Atmos Sci 67:1420–1437